Photoemission electron microscopy of diindenoperylene thin films

M. B. Casu,[1] I. Biswas,[1] M. Nagel,[1] P. Nagel, S. Schuppler,[2] and T. Chassé[1]
[1]*Institute of Physical and Theoretical Chemistry, University of Tuebingen, Auf der Morgenstelle 8, 72076 Tübingen, Germany*
[2]*Forschungszentrum Karlsruhe, Institut für Festkörperphysik, Postfach 3640, 76021 Karlsruhe, Germany*
(Received 11 December 2007; revised manuscript received 18 July 2008; published 13 August 2008)

We present the results of photoemission electron microscopy investigations of diindenoperylene thin films deposited by organic molecular-beam deposition on polycrystalline gold at room temperature. Our findings revealed the existence of a different molecular orientation, besides the already known λ and σ phases, characterized by an intermediate tilt angle. In thicker film regions, the energy of the films is minimized by a molecular arrangement that has an asymptotic tendency to the upright standing position. We have interpreted our results by using basic concepts in terms of relative strength of the substrate-molecule and molecule-molecule interactions.

DOI: 10.1103/PhysRevB.78.075310 PACS number(s): 73.20.−r, 71.20.Rv

I. INTRODUCTION

Organic materials have been extensively investigated in the recent decades. They were considered very appealing not only from a purely academic interest as a new class of materials but also because of their promising properties toward potential electronic applications. Nowadays organic-based displays are widely present on the market, used for hi-fi systems in cars, mp3 players, and mobile phones, as well as in television screens, or in e-paper, one of their most fascinating applications.

In the future they could change our vision of all those applications where a display or decorative lighting is required and even open new ways to use electronics. Therefore, it is very important to reach a general understanding of their electronic, structural, and morphological properties. Diindenoperylene (DIP, $C_{32}H_{16}$) is a perylene-based molecule that shows very high hole mobility already in thin films,[1] good film forming properties, and thermal stability.[2,3] Its use as an active layer in a device could give the opportunity to reach very good performance and long lifetime.

A general property that has been found investigating the growth of organic materials is their polymorphism.[4] Perylene single crystals (perylene is the core molecule of DIP) exist under two different crystalline forms: the α and the β one. Both of them belong to the monoclinic space group $P2_1/a$.[5,6] While the α form has a dimeric structure and four molecules in the unit cell,[5] the β one is monomeric and its unit cell contains two molecules.[6] Thiophene single crystals, a widely investigated molecule, also show two crystallographic phases depending on the growth temperature.[7,8] Polymorphism, basically due to several reasons such as the large dimension of the unit cell in comparison with inorganic materials and the anisotropy of the intermolecular interaction, is emphasized in film growth. One molecule when incorporated into thin films can give rise to different film polymorphs depending essentially on substrates (including its local morphology), preparation conditions, and thickness grown.[9–12] A systematic study of perylene deposited on an oxidized substrate revealed the existence of different molecular orientations depending on the growth parameters, both in monolayers and in multilayers.[10] Pentacene films deposited on Cu(110) show different phases depending on the actual film thickness.[13] In a monolayer regime molecules form a highly ordered commensurate structure with a planar adsorption geometry. For thin films a second phase is observed which is characterized by a tilting of the molecular plane of about 28°. Finally, exceeding a thickness of about 2 nm, films grow with an upright molecular orientation, leading to the formation of crystalline films which are epitaxially oriented with respect to the substrate.[13] A similar behavior has been shown investigating pentacene films deposited on Au(110).[14]

Two main polymorphs have been identified in DIP thin films depending on the substrate: an upright standing configuration (σ phase) when grown on rubrene and SiO_2 (Ref. 15) and a flat lying configuration (λ phase) when deposited on polycrystalline gold (Fig. 1).[16] Films deposited on sapphire show the coexistence of both phases.[15] The occurrence of the σ or λ phase depends not only on the substrate but also on the film preparation. Modulating the deposition conditions, one of the two phases can be favored. The nucleation of λ phase on top of σ phase is evident in DIP films grown on SiO_2 keeping the substrate temperature below 303 K.[15] DIP has been investigated with a variety of techniques including x-ray diffraction, atomic force microscopy (AFM), transmission electron microscopy (TEM), and ultraviolet photoelectron spectroscopy (UPS).[2,3,15,16] However, no soft x-ray spectromicroscopy has been used to correlate the electronic structure with the morphology and the structure of the film.

In this work we present the results of photoemission electron microscopy (PEEM) and x-ray photoelectron spectros-

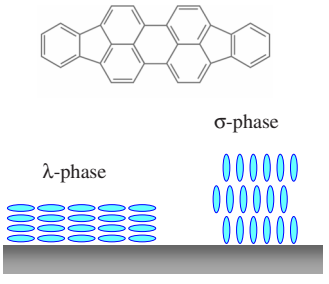

FIG. 1. (Color online) Schematic drawing of λ and σ phases. The DIP molecular structure is also shown.

copy (XPS) investigations on DIP thin films deposited on polycrystalline gold. PEEM is a very powerful tool that can give a deep insight in *in situ* growth.[12,17] In addition, the opportunity to use a synchrotron-radiation source allows the simultaneous investigation of morphology, structure, and electronic characteristics.

The paper is organized in the following way. First, we describe the experimental setup. We report the film topography observed by using a mercury high-pressure lamp, XPS growth investigations, and the morphology related to the electronic structure in Sec. III. The analysis and discussion of the molecular orientation derived from PEEM measurements for different film regions are presented in Sec. IV.

II. EXPERIMENTAL SECTION

The experiments were performed at Institut für Festkörperphysik (IFP) soft x-ray dipole beamline WERA at ANKA (Karlsruhe, Germany). This beamline covers photon energies that range from 100 to 1500 eV, with an energy resolving power of $E/\Delta E$ up to 10 000. The preparation chamber (base pressure of 2×10^{-10} mbar) is equipped with ion sputter guns, separated gas dosing systems, low energy electron-diffraction (LEED) optics, a quartz microbalance, and a homemade evaporation cell allowing organic molecular-beam deposition (OMBD). The spectroscopy main chamber is equipped with a SCIENTA SES2002 electron energy analyzer for photoemission spectroscopy. The PEEM chamber is equipped with a FOCUS-PEEM (FOCUS GmbH, Germany) and a mercury high-pressure lamp. The geometry of the PEEM experiment is fixed; the angle between the sample surface and the incident photon energy is 25°. The effective lateral resolution of the experiment with synchrotron radiation corresponding to the chosen field of view is about 300 nm. The energy resolution of the micro-near-edge x-ray absorption fine-structure (μ-NEXAFS) spectroscopy experiment was 0.140 eV and the polarization degree was 0.80. We also carried out standard NEXAFS measurements (energy resolution of ~0.095 eV and $P=0.95$) in the partial electron yield mode in grazing incidence ($\theta_2=70°$) and normal incidence ($\theta_1=0°$), taking advantage of the dependence of the NEXAFS spectra on the polarization of the incident radiation in order to investigate the molecular orientation.[18] NEXAFS and μ-NEXAFS spectra were normalized according to Refs. 19 and 20.

A gold foil (Goodfellow, purity 99.99%) was cleaned in ultrahigh vacuum (UHV) by means of repeated cycles of Ar sputtering and checked by using XPS. DIP was purified by thermal gradient sublimation and deposited in UHV conditions onto polycrystalline gold by using OMBD *in situ*. The nominal thickness was determined by using a quartz microbalance and cross-checked by using the attenuation of the XPS substrate signals (Au 4*f*). Furthermore, we probed the homogeneity and thickness of the films on a global as well as on a local scale by using XPS. Deposition rate (Φ) and substrate temperature (T_{sub}) were kept constant for each film preparation ($\Phi=3$ Å min^{-1}, $T_{sub}=$RT), leading to films characterized by grain size >60 nm.[21] All samples were carefully checked for radiation damage during beam exposure on the time scale of the single measurement (~1 h).

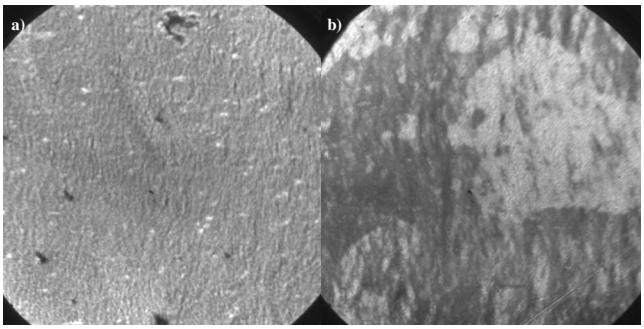

FIG. 2. Two typical images of the surface of a 12 nm thick DIP film. The field of view is 130×130 μm^2. The images were obtained in work-function contrast mode by using a mercury high-pressure lamp.

III. RESULTS

A. Topography

Figures 2(a) and 2(b) show two typical images of the surface of a 12 nm thick DIP film (the field of view is 130×130 μm^2) obtained with a mercury high-pressure lamp (Hg lamp). They show bright and dark regions which can be interpreted by the work function of the system.[12] In particular, the photon energy of the Hg lamp is 4.9 eV, the work function of Au is 5.2 eV, while the ionization potential of DIP thick films is 5.8 eV.[16] In addition, it has been shown that the work function of DIP deposited on polycrystalline gold does not change with the thickness, above the first three layers.[16] Thus, since the work function of Au is very close to the photon energy of the Hg lamp (the spectral line of the lamp is broad), the main contributions to the images come from the substrate. With increasing film thickness, these contributions will be attenuated by elastic and inelastic scatterings of the substrate photoelectrons, giving a dark contrast. First, we can immediately derive that the presence of a different brightness means a different contrast, implying that the films are rough. Second, we can assume that the darker regions reflect a contribution coming from zones with a different local thickness of the film. We can therefore conclude from the topographic investigation that the films are characterized by an inhomogeneous coverage. The work-function contrast is only one of many aspects that influence electron emission, for example, a possible source of contrast may also be due to the substrate topography. We cannot exclude contributions of this nature now, but a comparison with PEEM images (see next paragraph) obtained with synchrotron radiation may help us to distinguish them if present. To cross-check this finding we have also investigated the films by using XPS in normal emission (Fig. 3). In case of a perfect layer-by-layer growth, for the nominal thickness of 12 nm, the substrate should be perfectly covered and there should be no detection of the emitted photoelectrons coming from the gold substrate. Using an incident photon energy of 320 eV, only photoelectrons with very low kinetic energy (those

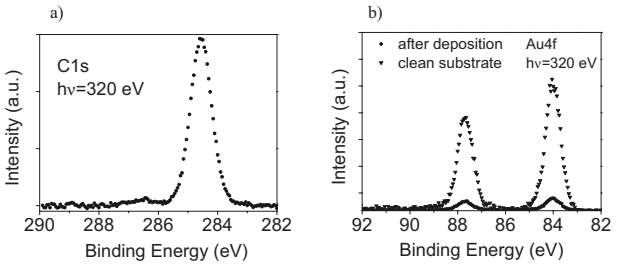

FIG. 3. Core level photoemission spectra: (a) C 1*s* XPS and (b) Au 4*f* XPS data of the clean substrate and after 12 nm DIP deposition, taken at a photon energy of 320 eV.

emitted from gold have kinetic energy of around 235 eV), corresponding to short inelastic mean-free path, can escape.[22] Despite the presence of a strong C1*s* signal due to the deposited DIP film [Fig. 3(a)] the Au 4*f* features (substrate intensity) in the XPS spectrum [Fig. 3(b)] are still relevant. A complete set of thickness-dependent XPS investigations has been performed showing the occurrence of a Stranski-Krastanov growth mode, in which at the beginning few layers grow layer by layer and then island growth starts.[23]

B. Morphology and electronic structure

PEEM images obtained with synchrotron radiation corresponding to the region shown in Fig. 2(b) are shown in Fig. 4 (the field of view is 130×130 μm^2). Each frame corresponds to different photon energies as indicated. We have recorded a set of frames in 0.15 eV steps of the photon energy at the C 1*s* edge between 280 and 330 eV. By overlapping each frame along the direction of increasing photon energy and looking at the intensity of the emitted photoelectrons for the single pixel, the μ-NEXAFS spectra of the investigated region are obtained. Comparing the images obtained with the Hg lamp [Fig. 2(b)] and the synchrotron radiation (Fig. 4, the latter at 278 eV, i.e., below the absorption edge) they look very similar. Thus, we can now exclude effects of the substrate topography in the images shown in Fig. 2. Figure 5 shows a PEEM stack, integrated in the photon energy range between 280 and 320 eV, together with two non-normalized μ-NEXAFS spectra for two film regions as indicated. If we look at the two non-normalized μ-NEXAFS spectra [Figs. 5(a) and 5(b)] of a darker and a brighter region, we can observe that the contribution coming from the substrate in the pre-edge region (below ~285 eV) is weaker in the spectra of the darker regions [Fig. 5(b)]. This implies that they are characteristic of locally thicker film regions. Therefore, this supports the conclusion coming from the analysis of the work function presented in the previous paragraph: we find that darker regions are thicker film regions and brighter regions thinner ones, thus the films are not homogeneous (Fig. 4).

Figure 6 shows a PEEM stack, integrated in the photon energy range between 280 and 320 eV, corresponding to the region shown in Fig. 2(a), together with the normalized μ-NEXAFS spectra for three areas as indicated. They are representative of the 12 nm thick film surface, chosen depending on their different contrast. We see that the main features of the spectra are always present but their intensity varies. Two main groups of resonances dominate the spectra: the π^* region up to 288 eV and the σ^* region above 288 eV. The former are due to transitions from C1*s* levels of nonequivalent carbon atoms mainly to the lowest unoccupied molecular orbital (LUMO).[23]

NEXAFS is the appropriate technique to investigate the orientation of the molecules in a film. The spectral features exhibit strong polarization dependence that can be used to determine the molecular orientation from the observed dichroic behavior.[18] It can be directly shown from the dipole selection rules that for a vector-type orbital, i.e., an orbital that points in a specific direction, the resonance intensity along the direction of the dominant component of the incident electric field is given by

$$I \propto (\cos^2\theta \sin^2\alpha + 2\sin^2\theta \cos^2\alpha), \tag{1}$$

with α angle between the normal to the surface and the orbital and θ angle between the incident radiation and the normal to the surface. Measuring the intensity for two different polarization directions with respect to the surface, in normal (θ_1) and in grazing incidence (θ_2), it is possible to determine α from the following equation:

$$\frac{1}{\tan^2\alpha} = \frac{1}{2P}\left(P - \frac{1-q}{\sin^2\theta_2 - q\sin^2\theta_1}\right), \tag{2}$$

where P is the polarization degree and q is the ratio between the intensities of the chosen resonances for the two different polarizations,

$$q = \frac{I(\theta_2)}{I(\theta_1)}. \tag{3}$$

In this work, the geometry of the PEEM experiment is fixed, thus the spectra are obtained only for one direction of the polarized incident radiation and we cannot quantitatively determine the molecular orientation by using these data. To overcome this problem we also performed standard NEX-

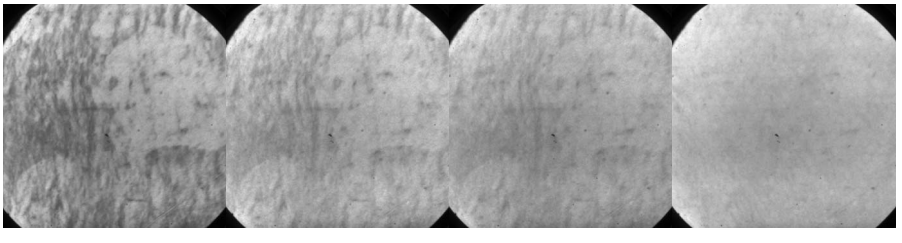

FIG. 4. PEEM images obtained with synchrotron radiation corresponding to the region shown in Fig. 2(b) (the field of view is 130×130 μm^2). Each frame corresponds to different photon energies as indicated.

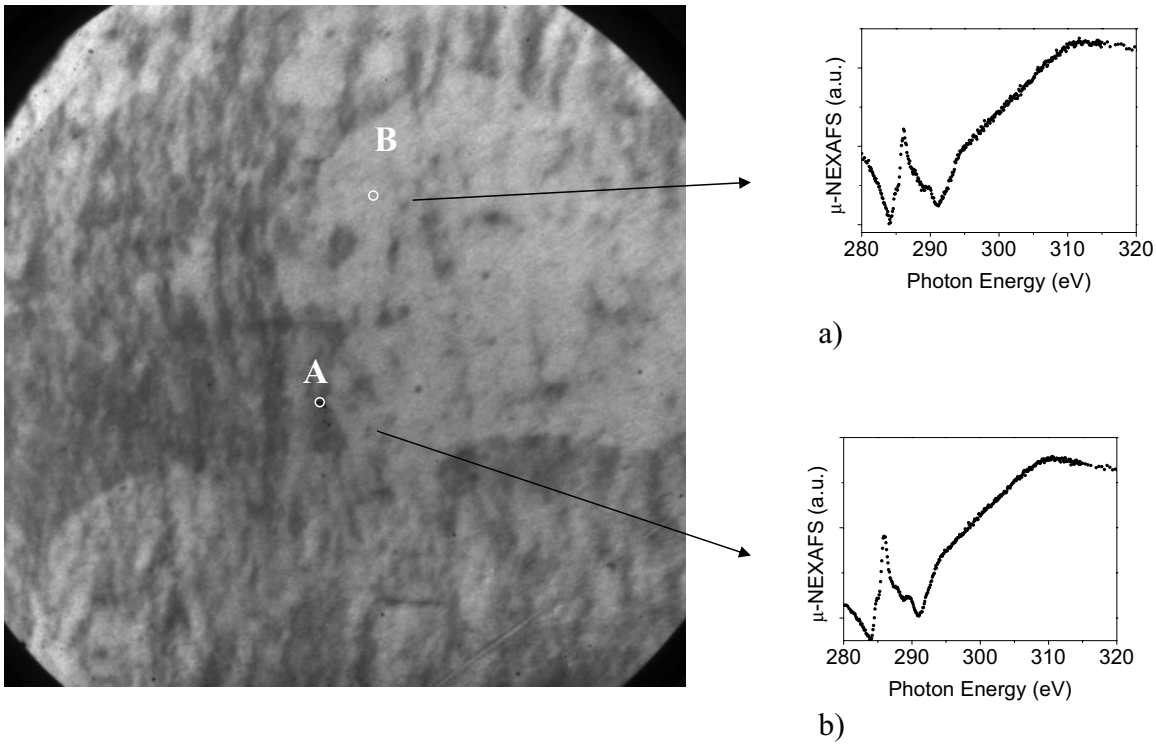

FIG. 5. PEEM stack, integrated in the photon energy range between 280 and 320 eV, together with two non-normalized μ-NEXAFS spectra [(a) and (b)] for two film regions as indicated.

AFS (Fig. 7) for two polarization directions and we were able to determine the molecular orientation according to Eq. (3). The obtained value is $47° \pm 5°$.

The θ_2 curve in Fig. 7 has been recorded for $\theta_2=70°$, i.e., the geometrical condition is therefore close to that of the PEEM experiment ($\theta=65°$, see Sec. II). Using the intensity of the main feature at around 286 eV (indicated with 2 in Figs. 6 and 7) as a reference and its relative variation with respect to the intensity of the σ^* region at 300 eV (I_2/I_{σ^*} ratio ~ 2), we can deduce some information about the local molecular arrangement by directly comparing μ-NEXAFS and standard NEXAFS spectra. This can be done for each pixel of the PEEM images and it is obviously a meaningful procedure only when the spectra are all normalized, as we did, according to Refs. 19 and 20.

Every μ-NEXAFS spectrum belonging to a given photon energy scan has been collected under the same experimental condition; thus any change in the spectral features is due to a change in the film structure. To use these spectra as a reference, first, we describe an appropriate framework in order to predict how the spectra should look like for different molecular orientations. A different alignment of the molecular orbital with respect to the incident electric-field vector implies different resonance intensities.[18] Let us examine two extreme cases taking into account only π^* resonances. If the molecules are flat lying on the surface the angle between the electric-field vector and the orbital is smaller than in our reference: the π^*-resonance intensities should be stronger and the I_2/I_{σ^*} ratio even more favorable to I_2. The opposite should be expected when comparing spectra coming from regions with upright standing molecules because the angle between the electric-field vector and the molecular orbital is larger than 47°. Now that we have built a reference interpretation for the μ-NEXAFS, we discuss this point in detail for the three regions (A–C) in Fig. 6. In Fig. 6(a), feature 2 is intense and comparable with the corresponding one in the θ_2 curve (see Fig. 7). The I_2/I_{σ^*} ratio is also very similar (~ 2.3), thus we can assume that the molecular orientation in region A resembles that of the average value 47°. Looking at the μ-NEXAFS spectrum belonging to region B [Fig. 6(b)], we observe that the main characteristics remain unchanged. Feature 2 still has a high intensity and the I_2/I_{σ^*} (~ 2.2) ratio is still favorable to the π^* resonances. This leads to the consequence that also in regions with characteristics like B, the molecular orientation is close to the value determined by using standard NEXAFS. However, there is a change in the electronic structure underlined, e.g., by the stronger intensity of feature 5. Finally, the strongest changes are revealed by the region C spectrum [Fig. 6(c)]. The relative intensities in the μ-NEXAFS spectrum are different and the I_2/I_{σ^*} ratio (~ 1) is more favorable to the σ^* resonances with respect to the previous regions. The orientation of the molecular axis is drastically changed indicating that the molecules in this region have a position closer to the upright standing one. Other details of the spectra have also changed indicating local differences in the electronic structure. We observe that different details in the electronic structure correspond to a different short-range order in the film, i.e., to different mutual molecular interaction, due to the different film morphology and to the environment seen from the molecules.

IV. DISCUSSION

It has been already shown that during growth different parameters play a fundamental role in determining the prop-

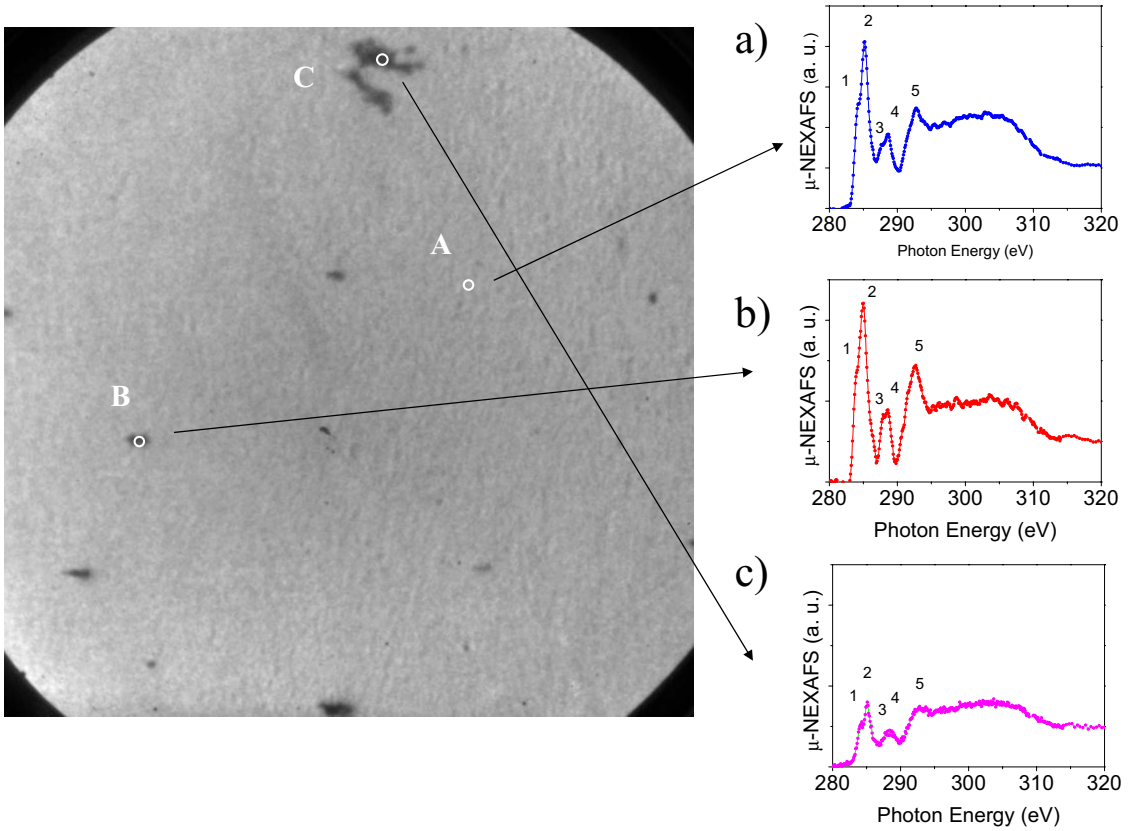

FIG. 6. (Color online) PEEM stack, integrated in the photon energy range between 280 and 320 eV, corresponding to the region shown in Fig. 2(a), together with normalized μ-NEXAFS spectra [(a)–(c)] for three representative regions as indicated. The μ-NEXAFS spectra have the same scale to facilitate the comparison.

erties of the films: preparation conditions, i.e., substrate temperature, deposition rate, and nature or type of substrates, determine different structural properties such as morphology and molecular orientation.[4,9–17,24–28] In this work we kept all parameters constant during preparation (Φ=3 Å min^{-1}, T_{sub}=RT) and we used only one material as substrate intending to limit the number of variables and thus to completely characterize the obtained model system DIP deposited on Au at room temperature. Our attention was especially focused on the possible occurrence of different molecular orientations even under those strictly determined preparation conditions. We have obtained an average molecular orientation of 47° for DIP films thickness above 10 nm. Still the molecular orientation calculated by using standard NEXAFS is averaged over the probed area (here about 0.9 mm diameter). Thus an angle of 47° may represent a critical value: we can imagine a scenario where at the surface half of the investigated domains present exactly upright standing molecules and the remaining half flat lying molecules. The presence of such domains in the investigated area with a wide range of different molecular orientations cannot be detected by standard NEXAF. However, the powerful aspects of μ-NEXAFS spectroscopy are preserved allowing for a high lateral resolution (in our experiment: 300 nm). This enables, within the limit of the lateral resolution, to look at the μ-NEXAS spectra picked up from different microregions of the same sample and to determine whether it is possible that adjacent domains, also within the same region of bright or dark areas, show different phases. Observing PEEM images and μ-NEXAS spectra we can deduce that the morphological and structural properties of the films are constant for large regions (at least 130×130 μm^2 field of view, see, for example, Fig. 6). In addition, they are very similar for film regions with analogous morphology. Region A has been chosen because it shows the predominant morphology of our films (see the contrast in Figs. 4 and 6). As discussed in the previous paragraph the estimated molecular orientation and the electronic structure of region A are in agreement with the

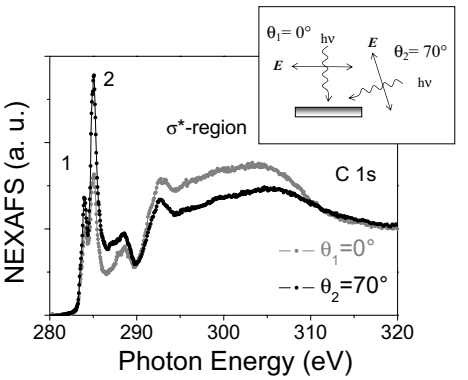

FIG. 7. C 1s standard NEXAFS spectra for a 12 nm thick film. They were taken in grazing (black curve) and in normal (gray curve) incidences. The geometry of the experiment is shown in the inset.

standard NEXAFS results. Examining further the film we select region B. Comparing regions A and B we observe that, despite the strong contrast between the two regions, their μ-NEXAFS spectra have very close characteristics [see Figs. 6(a) and 6(b)] and again a good similarity with the standard NEXAFS spectra. As mentioned, two phases have been identified for DIP grown on different substrates: σ phase (upright standing molecules) and λ phase (flat lying molecules).[15,16] This could lead to the idea that the hypothetic scenario with the two phases present in our films in the same concentration is the correct one. It cannot be ruled out when relying only on the standard NEXAFS investigations. With our comparison between standard and μ-NEXAFS spectra, we obtain evidence for an arrangement of the molecules in both regions A and B with their axis forming an angle of around 47° with respect to the substrate. Sampling randomly the surface, we have always obtained very similar μ-NEXAFS spectra, i.e., same molecular arrangement, in those regions with morphological characteristics like A or B. This value has now a different relevance than the one obtained by standard NEXAFS spectroscopy: it is not anymore averaged on a large area but it comes from well-defined microareas of the samples. We can rule out the possibility of the mentioned scenario (half upright standing molecules/half flat molecules), also in agreement with previous works where the content of σ phase has been estimated to be up to 26% throughout a 30 nm thick film.[16]

Parallel to this work, we also used the information delivered by standard NEXAFS investigations on DIP monolayer deposited on gold, where we saw that the molecules are flat lying on the substrate surface.[23] As soon as the thickness exceeds a couple of layers the molecules assume a position with their axis tilted with respect to the surface.[23] These observations are not surprising. It seems that DIP molecules behave very similarly to other organic materials such as pentacene deposited on Au(111) (Ref. 14) or phthalocyanines on polycrystalline gold, which show analogous behaviors.[27] Our PEEM results do not contain the information about the first monolayer and the buried layers since the maximum probing depth is about 10 nm. Therefore, the tilt of the molecular axis is a real effect and not an artifact due to the technique.

Our analysis shows that the film properties are completely dominated by the relative strength of substrate-molecule and molecule-molecule interactions.[25] In the monolayer regime, the interaction between the substrate and the molecules is strong enough to force the molecules in a flat lying configuration. DIP molecules are physisorbed on gold,[23] and the substrate acts as a template for the organic layers as long as the interaction substrate molecule is strong enough, i.e., for a couple of layers. Then it is overwhelmed by the molecule-molecule interaction. This picture is also supported by the evidence for a Stranski-Krastanov growth mode (layer plus islands), as we obtained from the PEEM investigation combined with XPS. At the beginning the substrate is covered by a couple of monolayers, then three-dimensional (3D) nucleation starts to be predominant, in agreement with a decrease in the interaction strength between the substrate and the layers after the first one, leading to the formation of 3D islands. So far, we have completely excluded from our discussion region C (see Fig. 6). Let us address which contribution the presence of such regions brings to the proposed picture. Region C has a very strong contrast in comparison with the neighboring film environment. (Note that label C does not indicate the complete darker area in the upper part of the image in Fig. 6 but only the region surrounded by the circle. The outside region shows a contrast similar to region B.) According to what we observed in the previous paragraph, this indicates that region C is locally thicker than regions like A and B. Actually it is the darkest and therefore the thickest region present in Fig. 6. We have seen that in this case the molecular orientation and the electronic structure are drastically changed. In particular, in region C the estimated molecular orientation is closer to the upright position than in any other investigated region of Fig. 6 [see Fig. 6(c)]. This agrees very well with our interpretation of the results in terms of a stronger influence of the molecule-molecule interaction when increasing the thickness. The energy of the films is minimized by a molecular arrangement that has an asymptotic tendency to the upright standing position. A complete crystallographic characterization of a DIP single crystal is still missing but it would be very interesting to compare the molecular orientation in thin films with that in single crystals. It may be possible that the molecular orientation in thicker films reproduces or tends to that one in the single crystal like in perylene thick films.[10] This would give a hint about the stability of the various molecular arrangements and which kind of geometry they represent with respect to the substrate.

Dürr *et al.*[16] already showed, with x-ray scattering, that for a 30 nm thick film deposited on gold the λ phase occurs in coexistence with the σ phase showing a concentration up to 26%. Our results evidence an intermediate molecular orientation with respect to the surface. While it is clear the tendency to the upright standing position in thicker regions, a real λ phase can be found only for very thin films (few layers). The results in both works can be explained in terms of substrate-molecule versus molecule-molecule interactions, the only dissimilar point is the arrangement of the molecules in the films. In our opinion, this difference has a main reason the different substrate preparations. The comparison of the two works shows how substrate defects and local morphology, in this specific case the roughness of the substrate, have a strong influence in terms of molecular orientation. In fact, we could not detect the same molecular arrangement as on evaporated polycrystalline gold.[16] This interpretation is also in agreement with Marchetto *et al.*[12] that found a strong dependence on the substrate morphology of perylene-tetracarboxylicacid-dianhydride (PTCDA) thin-film properties. The relevance in device engineering is obvious: a different preparation of polycrystalline gold, often used as an electrode, could imply different device performances for the same structure and active layer.

V. SUMMARY AND CONCLUSIONS

The presented PEEM results represent the x-ray spectromicroscopy study of DIP providing information on the occurring molecular orientation. Our investigations revealed

(1) the existence of a different molecular orientation (within the limit of the experimental resolution), beside the already known λ phase and σ phase, characterized by an intermediated tilt angle. In thicker film regions, the energy of the films is minimized by a molecular arrangement that has an asymptotic tendency to the upright standing position. (2) The growth mode is of the Stranki-Krastanov type. (3) DIP films show large orientational domains. We have interpreted our findings by using basic concepts in terms of relative strength of the interaction substrate molecule and molecule-molecule.

ACKNOWLEDGMENTS

The authors would like to thank the Angstroemquelle Karlsruhe ANKA for providing beam time at the soft x-ray beamline WERA, Jens Pflaum (University of Stuttgart) for valuable information, Frank Schreiber (University of Tübingen) for supplying highly purified diindenoperylene, and John E. Wong (University of Aachen) for reading the paper. Financial support by Ministerium für Wissenschaft, Forschung und Kunst Baden-Württemberg under Contract No. AZ 24-7532.23-21-18/2 is gratefully acknowledged.

[1] N. Karl, Synth. Met. **133-134**, 649 (2003).
[2] A. C. Dürr, F. Schreiber, M. Kelsch, H. D. Carstanjen, and H. Dosch, Adv. Mater. (Weinheim, Ger.) **14**, 961 (2002).
[3] S. Sellner, A. Gerlach, F. Schreiber, M. Kelsch, N. Kasper, H. Dosch, S. Meyer, J. Pflaum, M. Fischer, and B. Gompf, Adv. Mater. (Weinheim, Ger.) **16**, 1750 (2004).
[4] F. Schreiber, Phys. Status Solidi A **201**, 1037 (2004), and references therein.
[5] A. Camerman and J. Trotter, Proc. R. Soc. London, Ser. A **279**, 129 (1963).
[6] J. Tanaka, Bull. Chem. Soc. Jpn. **36**, 1237 (1963).
[7] G. Horowitz, B. Bachet, A. Yassar, P. Lang, F. Demanze, J.-L. Fave, and F. Garnier, Chem. Mater. **7**, 1337 (1995).
[8] T. Siegrist, R. M. Fleming, R. C. Haddon, R. A. Laudise, A. J. Lovinger, H. E. Katz, P. M. Bridenbaugh, and D. D. Davis, J. Mater. Res. **10**, 2170 (1995).
[9] S. Kera, M. B. Casu, K. R. Bauchspieß, D. Batchelor, Th. Schmidt, and E. Umbach, Surf. Sci. **600**, 1077 (2006).
[10] M. B. Casu, A. Schöll, K. R. Bauchspieß, D. Hübner, Th. Schmidt, C. Heske, and E. Umbach (unpublished).
[11] L. Chkoda, M. Schneider, V. Shklover, L. Kilian, M. Sokolowski, C. Heske, and E. Umbach, Chem. Phys. Lett. **371**, 548 (2003).
[12] H. Marchetto, U. Groh, Th. Schmidt, R. Fink, H.-J. Freund, and E. Umbach, Chem. Phys. **325**, 178 (2006).
[13] S. Söhnchen, S. Lukas, and G. Witte, J. Chem. Phys. **121**, 525 (2004).
[14] G. Beernink, T. Strunskus, G. Witte, and Ch. Wöll, Appl. Phys. Lett. **85**, 398 (2004).
[15] S. Kowarik, A. Gerlach, S. Sellner, F. Schreiber, L. Cavalcanti, and O. Konovalov, Phys. Rev. Lett. **96**, 125504 (2006).
[16] A. C. Dürr, N. Koch, M. Kelsch, A. Rühm, J. Ghijsen, R. L. Johnson, J.-J. Pireaux, J. Schwartz, F. Schreiber, H. Dosch, and A. Kahn, Phys. Rev. B **68**, 115428 (2003).
[17] F. J. Meyer zu Heringdorf, M. C. Reuter, and R. M. Tromp, Nature (London) **412**, 517 (2001).
[18] J. Stöhr and D. A. Outka, Phys. Rev. B **36**, 7891 (1987).
[19] A. Schöll, Y. Zou, Th. Schmidt, R. Fink, and E. Umbach, J. Electron Spectrosc. Relat. Phenom. **129**, 1 (2003).
[20] J. Stöhr, *NEXAFS Spectroscopy* (Springer-Verlag, Berlin, 1998).
[21] B.-E. Schuster and M. B. Casu (unpublished).
[22] http://xdb.lbl.gov/ and references therein.
[23] M. B. Casu, I. Biswas, M. Nagel, B.-E. Schuster, P. Nagel, S. Schuppler, and T. Chassé, Appl. Phys. Lett. **93**, 024103 (2008).
[24] E. Umbach and R. Fink, in Proceedings of the International School of Physics ''Enrico Fermi'' Course CXLIX, edited by V. M. Agranovich and G. C. La Rocca (IOS, Amsterdam, The Netherlands, 2002), p. 233.
[25] G. Witte and C. Woll, J. Mater. Res. **19**, 1889 (2004), and references therein.
[26] L. Zhang, H. Peisert, I. Biswas, M. Knupfer, D. Batchelor, and T. Chassé, Surf. Sci. **596**, 98 (2005).
[27] H. Peisert, I. Biswas, L. Zhang, M. Knupfer, M. Hanack, D. Dini, D. Batchelor, and T. Chassé, Surf. Sci. **600**, 4024 (2006).
[28] H. Peisert, I. Biswas, L. Zhang, M. Knupfer, M. Hanack, D. Dini, M. J. Cook, I. Chambrier, T. Schmidt, D. Batchelor, and T. Chassé, Chem. Phys. Lett. **403**, 1 (2005).